Free Radical Biology and Medicine 53 (2012) 1004–1015

Contents lists available at SciVerse ScienceDirect

Free Radical Biology and Medicine

journal homepage: www.elsevier.com/locate/freeradbiomed

Original Contribution

# Biophysical properties and cellular toxicity of covalent crosslinked oligomers of α-synuclein formed by photoinduced side-chain tyrosyl radicals

Claudio D. Borsarelli [a,b,*], Lisandro J. Falomir-Lockhart [b], Veronika Ostatná [c], Jonathan A. Fauerbach [d], He-Hsuan Hsiao [e], Henning Urlaub [e,f], Emil Paleček [c], Elizabeth A. Jares-Erijman [d,1], Thomas M. Jovin [b]

[a] Laboratorio de Cinética y Fotoquímica, Centro de Investigaciones y Transferencia de Santiago del Estero (CITSE-CONICET), Universidad Nacional de Santiago del Estero, RN 9 Km 1125, 4206 Santiago del Estero, Argentina
[b] Laboratory of Cellular Dynamics, Max Planck Institute for Biophysical Chemistry, Am Fassberg 11, 37077 Goettingen, Germany
[c] Institute of Biophysics, Academy of Sciences of the Czech Republic, v.v.i., Královopolská 135, 612 65 Brno, Czech Republic
[d] Departamento de Química Orgánica, Facultad de Ciencias Exactas y Naturales, Universidad de Buenos Aires, CIHIDECAR CONICET, Buenos Aires, Argentina
[e] Laboratory of Bioanalytical Mass Spectrometry, Max Planck Institute for Biophysical Chemistry, Am Fassberg 11, 37077 Goettingen, Germany
[f] Bioanalytics, Department of Clinical Chemistry, University Medical Center Goettingen, Robert Koch Strasse 40, 37075 Goettingen, Germany

ARTICLE INFO

*Article history:*
Received 12 March 2012
Received in revised form
20 June 2012
Accepted 25 June 2012
Available online 6 July 2012

*Keywords:*
Parkinson's disease
Neurodegeneration
Oxidative stress
Photocrosslinking
SH-SY5Y
Protein aggregation
Protein photooxidation

ABSTRACT

Alpha-synuclein (αS), a 140 amino acid presynaptic protein, is the major component of the fibrillar aggregates (Lewy bodies) observed in dopaminergic neurons of patients affected by Parkinson's disease. It is currently believed that noncovalent oligomeric forms of αS, arising as intermediates in its aggregation, may constitute the major neurotoxic species. However, attempts to isolate and characterize such oligomers in vitro, and even more so in living cells, have been hampered by their transient nature, low concentration, polymorphism, and inherent instability. In this work, we describe the preparation and characterization of low molecular weight covalently bound oligomeric species of αS obtained by crosslinking via tyrosyl radicals generated by blue-light photosensitization of the metal coordination complex ruthenium (II) tris-bipyridine in the presence of ammonium persulfate. Numerous analytical techniques were used to characterize the αS oligomers: biochemical (anion-exchange chromatography, SDS-PAGE, and Western blotting); spectroscopic (optical: UV/Vis absorption, steady state, dynamic fluorescence, and dynamic light scattering); mass spectrometry; and electrochemical. Light-controlled protein oligomerization was mediated by formation of Tyr–Tyr (dityrosine) dimers through –C–C– bonds acting as covalent bridges, with a predominant involvement of residue Y39. The diverse oligomeric species exhibited a direct effect on the in vitro aggregation behavior of wild-type monomeric αS, decreasing the total yield of amyloid fibrils in aggregation assays monitored by thioflavin T (ThioT) fluorescence and light scattering, and by atomic force microscopy (AFM). Compared to the unmodified monomer, the photoinduced covalent oligomeric species demonstrated increased toxic effects on differentiated neuronal-like SH-SY5Y cells. The results highlight the importance of protein modification induced by oxidative stress in the initial molecular events leading to Parkinson's disease.



## Introduction

Parkinson's Disease (PD), the second most common neurodegenerative disorder, is characterized primarily by the functional loss of dopaminergic neurons in the *substantia nigra* of the midbrain [1]. The precise cause(s) of cell death are unknown, although misfolding and aggregation of the abundant neuronal protein α-synuclein (αS), featuring covalent and noncovalent linkages [2], are almost certainly involved in the pathogenesis of the disease [3–5]. αS is a small (140 amino acids, 14.5 kDa) negatively charged, natively disordered protein lacking a distinct secondary structure when free in solution [3], although recent reports suggest that αS may adopt a distinct conformation in vivo [6,7]. αS is the major component of

*Abbreviations:* αS, Alpha-synuclein; APS, ammonium persulfate; 1C3, anti-dityrosine specific antibody; syn211, anti-αS specific antibody; AFM, atomic force microscopy; CPS, chronopotentiometric stripping; DLS, dynamic light scattering; ESI-MS, electrospray ionization mass spectrometry; HMDE, hanging mercury drop electrode; HMWO, high molecular weight oligomers; LMWO, low molecular weight oligomers; PD, Parkinson's disease; PICUP, photoinduced crosslinking of unmodified proteins; ThioT, thioflavin-T; $Ru(bpy)_3^{2+}$, tris(bipyridine)ruthenium(II) cation

* Corresponding author at: Permanent address: Laboratorio de Cinética y Fotoquímica, Centro de Investigaciones y Transferencia de Santiago del Estero (CITSE-CONICET), Universidad Nacional de Santiago del Estero, RN 9 Km 1125, 4206 Santiago del Estero, Argentina. Fax: +54 385 4509528 (Int. 1797).
*E-mail address:* cborsarelli@yahoo.com.ar (C.D. Borsarelli).
[1] Deceased on September 29, 2011.

0891-5849/$ - see front matter © 2012 Elsevier Inc. All rights reserved.
http://dx.doi.org/10.1016/j.freeradbiomed.2012.06.035

intracellular aggregates formed by dense tangles of amyloid-like fibrils, usually denoted as Lewy bodies, which constitute the major pathological hallmark of affected neurons in PD patients [8].

Cellular oxidative stress is considered as one of the more relevant factors triggering protein aggregation and toxicity [9,10], probably initiating posttranslational modifications of proteins, as well as the oxidation of nucleic acids and lipids. Several in vitro studies of αS have shown the relevance of tyrosine residues to the oxidation-induced formation of covalent aggregates, in which stable covalent interprotein –C–C– bonds in the form of dityrosine (diTyr) groups are implicated [11,12]. DiTyr has also been identified as an oxidative stress marker in brain tissue models of PD [13].

The covalent crosslinking of proteins forming soluble oligomers may constitute nucleation platforms for further elongation and noncovalent deposition. Krishnan et al. [14] concluded that oxidative dimer formation is the critical rate-limiting step in fibrillogenesis, although it has also been reported that covalent oligomeric species reduce the yield of amyloid fibrils [15]. These results can be interpreted in the context of the sigmoidal behavior observed during the aggregation of αS in vitro, a process that is generally described by a nucleation-elongation model [16,17]. The duration of the lag phase that precedes the appearance of insoluble amyloid fibrils with the characteristic cross-β-sheet secondary structure depends on numerous factors such as protein concentration, buffer composition and pH, temperature, and the presence of interacting partners [17–19]. Amyloid fibril formation in vitro has been monitored by several methods [20], the most widely used being the change in thioflavin-T (ThioT) fluorescence upon binding to cross-β-sheet structures [21] and, more recently, by environmental sensitive probes indicating the transient occurrence of early aggregation intermediates [22–24]. Complementary AFM and cryo-EM tomography images also provide evidence for supramolecular prefibrillar forms of αS [25].

The fundamental questions are the identity of the molecular species responsible for cellular toxicity and the manner(s) in which they form. One possibility is that specific modifications of αS lateral chains perturb the normal interactions of αS and promote its pathological association(s) [10]. Considering that oxidative stress is one of the major factors linked to PD, oxidation of αS residues is a pathway to be considered. In previous studies, the specific oxidation of side-chain tyrosine of αS was achieved by peroxidative or peroxynitrile chemistry, leading to the formation of *n*-mers ($n \geq 2$) as well as lower molecular breakdown products [11,12,15,26,27]. Other oxidative stress models based on Fenton chemistry (i.e., a transition metal/$H_2O_2$ or enzyme/$H_2O_2$ systems) have also been extensively employed to reproduce in vitro αS covalent aggregation, but these systems are less specific in that they induce other modifications of amino acid residues, as in the case of $Cu^{2+} + H_2O_2$ [28]. In contrast, the involvement of tyrosine is essential in the peroxidative aggregation of αS induced by $H_2O_2$+ cytochrome *c*, but this process also yields αS degradation products and cytochrome *c*–αS adduct species [11]. In summary, the nature of the sources of reactive oxygen or nitrogen species (ROS and RNS, respectively) is a key feature of oxidation-induced aggregation.

An alternative that avoids both protein breakdown and unspecific reactions is the method of photoinduced crosslinking of unmodified proteins (PICUP) proposed by Fancy and co-workers [29,30]. This technique uses the tris(bipyridine)ruthenium(II) chloride complex ($Ru(bpy)_3Cl_2$) as a photosensitizer and ammonium persulfate (APS) as a sacrificial electron donor. The process is initiated by blue-light (e.g., 450 nm) absorption by the tris(bipyridine)ruthenium(II) cation ($Ru^{II}(bpy)_3^{2+}$) to produce the excited metal-to-ligand charge-transfer triplet state ($^*Ru^{II}(bpy)_3^{2+}$), (Eq. (1)). In the presence of persulfate anion ($S_2O_8^{2-}$), the electron-transfer quenching reaction of the excited complex occurs with diffusion-controlled rate constant ($k_q = 1.4 \times 10^9\ M^{-1}\ s^{-1}$) [31], generating the oxidized $Ru^{III}(bpy)_3^{3+}$, the sulfate radical anion $SO_4^{\bullet -}$, and nonreactive sulfate anion (Eq. (2)).

$$Ru^{II}(bpy)_3^{2+} + h\nu \rightarrow {}^*Ru^{II}(bpy)_3^{2+} \quad (1)$$

$${}^*Ru^{II}(bpy)_3^{2+} + S_2O_8^{2-} \xrightarrow{k_q} Ru^{III}(bpy)_3^{3+} + SO_4^{\bullet -} + SO_4^{2-}. \quad (2)$$

Both the $Ru^{III}(bpy)_3^{3+}$ and $SO_4^{\bullet -}$ species are potent one-electron oxidants capable of oxidizing primarily aromatic and sulfur-containing residues [32–34]. The reduction potentials of side-chain and backbone-derived radicals indicate that the ultimate sinks for oxidizing equivalents are Tyr, Trp, and Cys residues [35]. Wild-type αS lacks Cys and Trp, but has four tyrosines (Y39, Y125, Y133, and Y136). One assumes that photogenerated oxidant $Ru^{III}(bpy)_3^{3+}$ and $SO_4^{\bullet -}$ species would react with the Tyr residues to form side-chain tyrosyl radicals ((Eqs. (3) and (4)).

$$Ru^{III}(bpy)_3^{3+} + \alpha S\text{–Tyr} \xrightarrow{-H^+} Ru^{II}(bpy)_3^{2+} + \alpha S\text{–Tyr}^{\bullet} \quad (3)$$

$$SO_4^{\bullet -} + \alpha S\text{–Tyr} \xrightarrow{-H^+} SO_4^{2-} + \alpha S\text{–Tyr}^{\bullet}. \quad (4)$$

The reaction of $Ru^{III}(bpy)_3^{3+}$ with accessible Tyr residues of a protein restores the ground state of the sensitizer molecule, allowing its reutilization by photon absorption ((Eq. (3)) [29,30]. In turn, the reaction between two side-chain tyrosyl radicals of different protein molecules can form a Tyr–Tyr bridge via–C–C– bonds, generating the ortho-diTyr fluorophore after internal enolization [36] (Eq. (5)), which has a distinctive 405 nm emission band at neutral pH [37].

$$2\ \alpha S\text{–Tyr}^{\bullet} \xrightarrow{-H^+} \alpha S\text{–Tyr-Tyr}–\alpha S. \quad (5)$$

According to the PICUP mechanism [29], another crosslinking pathway could be via the coupling of a side-chain tyrosyl radical of a $Ru^{III}(bpy)_3^{3+}$ oxidized protein with one of several possible side-chain nucleophile amino acids (i.e., X=Tyr, Trp, Cys). Subsequent abstraction of a hydrogen atom by the sulfate radical consummates the reaction by forming covalent –C–X– bonds, the nature of which depends on the nucleophilic amino acid residue. In the case of αS, such reactions can only occur between available tyrosines residues ((Eqs. (6) and (7)).

$$\alpha S\text{–Tyr}^{\bullet} + \alpha S\text{–Tyr} \rightarrow \alpha S\text{–Tyr-Tyr}^{\bullet}–\alpha S \quad (6)$$

$$\alpha S\text{–Tyr-Tyr}^{\bullet}–\alpha S + SO_4^{\bullet -} \xrightarrow{-H} \alpha S\text{–Tyr-Tyr}–\alpha S + HSO_4^{-}. \quad (7)$$

The PICUP method has been applied to crosslink proteins whose native states are monomeric, homo-, or heterocomplexes [30], and to form low molecular weight oligomers of the Aβ peptide involved in Alzheimer's disease [38,39]. The advantage of this procedure, not shared by standard bifunctional crosslinker reagents, is the very high yield of crosslinked products obtained with very short irradiation times (e.g., seconds) and readily available visible light sources.

In this study we focused on the photoinduced oxidative formation of side-chain tyrosyl radicals of αS, as a controlled method for producing in vitro several stable covalent oligomeric species (dimers, trimers, …, *n*-mers). These species were monitored and characterized by SDS-PAGE, optical spectroscopy (UV/Vis absorption, steady state and dynamic fluorescence, and dynamic light scattering), electrochemistry, mass spectrometry, and atomic force microscopy. The purified size-specific oligomeric covalent species were tested for their influence on the kinetics of in vitro amyloid fibril formation and their capacity for inducing cytotoxicity on exposure to differentiated SH-SY5Y cells, in the latter case as a potential relevant model for processes underlying the response(s) to biological oxidative stress.

## Materials and methods

### Materials

All chemicals were analytical purity grade products of Sigma Chemical Co. (St. Louis, MO), and were used as received. All solutions were prepared using deionized water (Millipore, Milli-Q). Antibodies anti-diTyr (1C3) and anti-αS (syn211) were obtained from Antibodies-Online (Germany) and Abcam (UK), respectively.

### Methods

#### Protein expression and purification

Recombinant wild-type human αS was expressed in *Escherichia coli* using plasmid pT7-7 encoding for the protein sequence (courtesy of the Lansbury laboratory, Harvard Medical School, Cambridge, MA). The purification was based on the osmotic shock protocol described by Huang et al. [40] with some modifications. Details are described in the Electronic Supplementary Material (ESM). Protein purity was assessed by SDS-PAGE and electrospray ionization mass spectrometry (ESI-MS). The purified protein was stored at −20 °C. Prior to the photocrosslinking or other reactions, the protein stock solutions were ultracentrifuged for 90 min at 75,000 rpm (300,000*g*) at 4 °C in a Beckman TL-100 Ultramicrocentrifuge to remove microaggregates. The protein concentration was determined from $A_{275}$ using a molar extinction coefficient of 5600 $M^{-1}$ $cm^{-1}$ [41].

#### Photoinduced crosslinking of αS

The photoreactions were carried out in a 5 × 5-mm quartz fluorescence cuvette with 500 μL of a ~100 μM αS solution in air-saturated 25 mM Na-$PO_4$, pH 7.4, following a procedure similar to that of Fancy and co-workers [29,30]. The concentration of the photosensitizer $Ru(bpy)_3Cl_2$ was typically 15–45 μM, and in all cases, a 20-fold molar excess of the electron acceptor ammonium persulfate (APS) was present. The samples were placed in a cuvette holder with a magnetic stirrer, and irradiated with a Superlite SUV-DC illuminator (Lumatec, Germany) equipped with a 200 W DC super pressure short-arc Hg lamp. The output beam was conducted through a flexible light-guide and a 445 ± 30-nm bandpass filter (Chroma HQ445/60 M) to the sample. The irradiance of the incident beam was 2.2–2.4 mW $cm^{-2}$. The exposure time (5–500 s) was controlled with the timed shutter of the Superlite apparatus. At different times, and immediately after each irradiation, 5-μL aliquots of the samples were diluted in 25 μL of 1x gel loading buffer containing 1 mM dithiothreitol (DTT) to quench the radical reaction. Control samples lacking APS or light exposure were prepared and processed in parallel. The samples were heated to 95 °C for 5 min, and loaded on a 12% SDS NuPAGE precast gel (Invitrogen) for electrophoretic separation. The monomeric and oligomeric species of αS were visualized by staining with Coomassie brilliant blue. In parallel, the reaction progress was monitored by both UV–vis absorption and fluorescence spectroscopies (see below). The presence of diTyr residues was also demonstrated by Western blotting with a specific monoclonal antibody (1C3).

#### Purification of covalent oligomers

A 500-μL oligomeric mixture solution was prepared as indicated above by 200 s of blue-light irradiation. The mixture was quickly rendered free of sensitizer ions by passage through a PD10 column equilibrated with 30 mM Tris–HCl, pH 7.5. The sample was then applied to a MonoQ 4.6/100 PE anion-exchange column (GE Healthcare) in a Smart System (Pharmacia Biotech), and fractionated with a gradient of 150–500 mM NaCl. Fractions (500 μL) were collected and the protein concentration was estimated with the BCA Protein Quantization Kit (Pierce/Thermo Scientific). The fractions corresponding to the different oligomeric species were checked by SDS-PAGE before further characterization and use.

#### Characterization of covalent oligomers

In addition to monitoring the photocrosslinking reaction by SDS-PAGE and densitometry, the fully or partially fractionated oligomers were also characterized by the following techniques:

*UV–vis absorbance and fluorescence spectroscopies.* Spectra were registered with a Cary 100 spectrophotometer and a Cary Eclipse spectrofluorimeter (Varian, Australia), using a 45-μL fluorescence quartz cuvette with a pathlength of 3 × 3 mm (Hellma, Germany). Corrected excitation and emission spectra were acquired with a 5-nm bandwidth. Emission spectra were registered with excitation at 275 and 320 nm for selective excitation of Tyr or diTyr chromophores, respectively. Emission anisotropy measurements of diTyr were also performed with excitation at 320 nm.

*Mass spectrometry analysis.* A mixture of covalent aSyn oligomeric species, obtained by the $Ru(bpy)_3^{2+}/S_2O_8^{2-}$/light system, and wild-type monomer was digested with trypsin (1:20 enzyme to substrate mass ratio) and the resulting peptides were analyzed with a LTQ-Orbitrap Velos mass spectrometer (Thermo Fisher Scientific) operated in the data-dependent mode to automatically switch between MS and MS/MS acquisition. Details are described in the ESM.

*Fluorescence lifetime measurements.* Fluorescence decay times were measured in a Horiba/Jobin Yvon Fluorolog 3 spectrofluorimeter with double grating monochromators, TBX Picosecond Photon Detector modules, and a Single Photon Counting Controller, employing a NanoLED 320 (319 nm) and an excitation band filter FF01-320/40 (Semrock). Decays were recorded over 50 ns in 1024 channels. The anisotropy correlation times and lifetimes were calculated employing Mathematica (Wolfram Research, USA) [42], employing a solution of glycogen to evaluate the detector impulse response function.

*Dynamic light scattering (DLS).* Particle size estimation was performed using a 45-μL quartz cuvette (Hellma, Germany) with a Zetasizer Nanoseries (Malvern Instruments, UK), employing a 633-nm laser and the detector in the backscattering configuration. Decays of photon correlation were fitted employing the built-in software with the CONTIN routine. The results were represented in the form of a histogram showing the contribution of each size interval to the overall scattering of the sample.

*Electrochemistry.* Electrochemical measurements were performed with a μAUTOLAB Analyzer (EcoChemie, The Netherlands) in combination with a VA-Stand 663 hanging mercury drop electrode (HMDE) as working electrode (Metrohm, Herisau, Switzerland). The standard three-electrode cell was used, with an Ag|AgCl|3 M KCl electrode as the reference electrode and a platinum wire as the auxiliary electrode. All experiments were carried out at room temperature under air. A 50 mM Na-PO4 buffer (pH 7.0) was used as the supporting solution. A 300 nM protein (full electrode coverage for monomeric αS) was adsorbed at the working electrode for accumulation time, $t_A$ 60 s, at accumulation potential, $E_A$ -0.1 V (unless stated otherwise); followed by application of the stripping current to HMDE and recording of the $E$–$t$ curve, which was automatically converted to $(dE/dt)^{-1}$–$E$. Initial potential, $E_i = E_A$; final potential $E_f = -1.955$ V; stripping current, $I_{str} = -7$ μA. Alternatively, the dependence on

the polarization potential $E$ of the specific differential capacity ($C_s$) of the electrode double layer of αS-modified HMDE was determined. $C_s$–$E$ curves were recorded to monitor the protein adsorption/desorption behavior. For the determination of the differential capacity, impedance measurements were conducted at 237 Hz with 10 mV amplitude. The specific capacity, $C_s$, was calculated for a HMDE area of 0.4 $mm^2$.

*Aggregation kinetics of αS*

To analyze the effect of the covalent oligomers on amyloid fibril formation at 37 °C, two types of experiments were conducted. The first assay employed mixtures of wild-type αS (starting solution 100 μM protein) with oligomers formed in situ by blue-light photolysis of $Ru(bpy)_3^{2+}$ (15 μM) in the presence of $S_2O_8^{2-}$ (300 μM) for 20 s or 200 s. After photolysis of the samples, the protein mixture was separated from the sensitizer ions by ultrafiltration with Amicon microfilters (cutoff 10 kDa), washing with 30 mM Tris–HCl (pH 7.5) buffer.

The second assay involved the addition of 20 μM of different purified oligomeric species (dimers, tetramers, or oligomers) to 100 μM αS in 30 mM Tris–HCl (pH 7.5). The solutions were incubated in 5 × 5-mm quartz cuvettes with vigorous stirring using a magnetic bar. The aggregation kinetics of each sample was monitored by either the second-order static scattering of the excitation light (340 nm→680 nm) or by removal of small aliquots from the incubation solution at different time intervals and dilution to appropriate concentrations for the ThioT assay [24]. The aggregations curves were fitted to a nucleation-propagation model according to Eq. 8 [17]

$$Y_t = Y_0 + \Delta Y \frac{e^{k_{app}t} - 1}{e^{k_{app}t} + e^{k_{app}t_{1/2}} - 2} \quad (8)$$

in which $Y_t$ is the monitoring parameter (total light scattering or fluorescence intensity) as a function of the aggregation time, $\Delta Y = Y_{end} - Y_0$ is the difference between the final and initial values of the parameter indicating the extent of reaction, $t_{1/2}$ the time required to reach the midpoint of the rapid growth phase, and $k_{app}$ the apparent growth rate constant; $k_{app} = k_{agg}[\alpha S]$, with $k_{agg}$ the second-order rate constant for incorporation of the monomer into the growing amyloid fibrils.

*AFM measurements*

Atomic force microscopy (AFM) was performed with a Veeco Nanoscope Model IIIa using silicon nitride tips (μmash) of 10-nm radius and 300 KHz drive frequency for tapping mode imaging in air. Samples were diluted 10-fold with Milli-Q water and 10 μL of the diluted solution was spin-coated onto freshly cleaved mica of 0.5 $cm^2$.

*Cytotoxicity of covalent oligomers*

The cellular toxicity of the covalent oligomers was assessed by incubation of differentiated, SH-SY5Y cells with the preparations. Subconfluent cultures of SH-SY5Y cells were induced to differentiate by incubation with 10 μM retinoic acid (RA) in DMEM medium (Invitrogen), supplemented with 3% fetal calf serum and 1% penicillin/streptomycin for 10–12 day in 96-well plates. The purified oligomer fractions were diluted in DMEM+Hepes (phenol red-free) medium (Invitrogen) at different concentrations (1, 5, and 20 μM), added to the cells, and incubated for 40–44 h. Control conditions included addition of an equal concentration of monomeric wild-type αS and media plus buffer. Each well was washed twice with Hank's buffered saline solution and the metabolic rate was measured employing 10 μL of WST-1 Cell Proliferation Reagent (Roche Applied Science) per well in DMEM+Hepes (phenol red-free), following the instructions of the manufacturer. The oxidation of the reagent was monitored regularly in a PHERAStar FS microplate reader (BMG, Germany) by $A_{450}$ and $A_{690}$. The final recordings were taken before the controls reached saturation (~2.5 h).The cytotoxicity effect was estimated by comparison of the remaining relative metabolic capacity with that of the controls. The results were expressed as percentages of the remaining metabolic rate relative to that of cells incubated with unmodified monomeric αS.

## Results

*$Ru(bpy)_3^{2+}/S_2O_8^{2-}$-mediated photocrosslinking of αS*

Irradiation with blue light (445 ± 30 nm) for determined time periods of monomeric αS (14.4 kDa) solutions in the presence of the photosensitizer mixture $Ru(bpy)_3^{2+}/S_2O_8^{2-}$ resulted in the efficient generation of stable dimers, trimers, tetramers, …, *n*-mers (i.e., high molecular weight oligomers, HMWO) of the protein. The products were assigned by comparison with the molecular weight marker lane in the denaturing SDS-PAGE gel (Fig. 1a). The formation of the covalent-linked oligomeric species

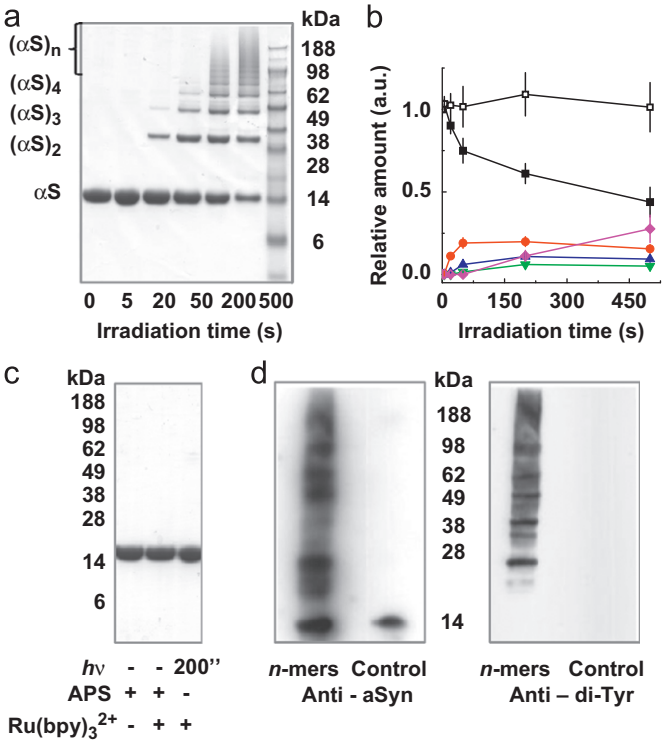


**Fig. 1.** Formation of oligomeric species of αS by photoinduced oxidation of Tyr residues: (a) Photo-initiated crosslinking of αS in phosphate buffer with $Ru(bpy)_3^{2+}/S_2O_8^{2-}$/light leads to efficient and progressive formation of oligomeric αS species as shown by the SDS-PAGE gel. (b) Kinetic profiles of the relative fractions of oligomeric species obtained from densitometric analysis of SDS-PAGE gel of panel a. The band areas of the oligomers were normalized by the stoichiometric factor corresponding to each species: (black squares) monomer αS; (red circles) dimers $(\alpha S)_2$; (blue up triangles) trimers $(\alpha S)_3$; (green down triangles) tetramers $(\alpha S)_4$; (magenta diamonds) high molecular weight oligomers $(\alpha S)_{n>4}$ averaged as hexamers ($n=6$). The open squares represent the sum of all species. (c) The formation of covalent oligomers of αS was only produced by the combination of $Ru(bpy)_3^{2+}/S_2O_8^{2-}$/light. The samples kept in dark were incubated for 30 min before being loaded on the gel. (d) Western blots of monomeric and photocrosslinked oligomeric species of αS formed in the presence of $Ru(bpy)_3^{2+}/S_2O_8^{2-}$/light irradiated for 200 s. The αS and the diTyr were sequentially detected employing the specific monoclonal antibodies syn211 (left panel) and 1C3 (right panel), respectively. Monomeric αS did not show detectable levels of diTyr in neither the control nor oligomeric mixture. (For interpretation of the references to color in this figure legend, the reader is referred to the web version of this article.)

was progressive and concomitant with the degradation of the monomeric αS (14.4 kDa), the band of which diminished in intensity in the analytical gels. SDS-PAGE revealed the formation of low molecular weight oligomers (LMWO): dimers [$(\alpha S)_2$, 28.8 kDa], trimers [$(\alpha S)_3$, 43.2 kDa], and tetramers [$(\alpha S)_4$, 57.6 kDa] during the first 50 s of photolysis, with dimers as the predominant intermediate species. At longer irradiation times, the unresolved spots at the top of the gel indicated the accumulation of additional HMWO species, i.e., $(\alpha S)_{n>4}$. Shorter peptides with MW < 14 kDa were not observed, indicating that the photo-induced reaction did not produce breakdown peptides of αS, as previously observed in the peroxidation of the protein with cytochrome $c+H_2O_2$ [15]. From densitometric analysis of the initial and final spots of the monomer αS, approximately 56% of the protein was converted to oligomeric species after 500 s of irradiation. The kinetic profiles of the relative amounts of each species were obtained by densitometry of the gel of the photo-crosslinked samples, in which the band areas of the oligomers were normalized by the respective stoichiometric factors (Fig. 1b). In the case of HMWO, i.e., $(\alpha S)_{n\geq 4}$, for which the bands in the gel were difficult to resolve, the total area was processed considering the mean species to be a hexamer, $(\alpha S)_6$. With the last assumption, the computations yielded total relative fractions of oligomeric species (open squares) ≈ 100% at all irradiation times. The consumption of monomeric αS (black squares) and the concomitant formation of dimers $(\alpha S)_2$ (red circles) were faster at the beginning of the reaction, with smilar initial rates of ~0.6 μM/s (expressed in monomer units). The accumulation of $(\alpha S)_2$ after 50 s of photocrosslinking led to formation of trimers $(\alpha S)_3$ (blue up triangles), and also of tetramers $(\alpha S)_4$ (green inverted triangles) albeit at a slower rate. After 150 s of photocrosslinking, the consumption of monomer was slower and similar to that observed for formation of the total HMWO considered as "hexamers." The lower rate can be attributed to reduced concentrations of monomeric protein and the slower diffusion of the reacting oligomeric species.

Covalent crosslinking of αS was not observed under dark conditions with protein solutions containing either the electron-acceptor $S_2O_8^{2-}$ alone or the $Ru(bpy)_3^{2+}/S_2O_8^{2-}$ mixture (left and center lanes in Fig. 1c), demonstrating that chemical crosslinking was not induced under either condition. Irradiation of αS solutions with $Ru(bpy)_3^{2+}$ in the absence of $S_2O_8^{2-}$ also failed to promote efficient protein crosslinking (right lane in Fig. 1c). Under this condition, the excited state of $Ru(bpy)_3^{2+}$ is efficiently quenched by molecular oxygen to produce singlet molecular oxygen ($^1O_2$) with a quantum yield of ~0.40 [43]. This reactive oxygen species reacts efficiently ($k_r \approx 10^6$–$10^8\ M^{-1}\ s^{-1}$) with electron-rich amino acids, e.g., Tyr, Met, and His, to yield side-chain oxidation products such as endo- and hydroperoxides [35,44]. In the present case, this potential $^1O_2$-mediated oxidation reaction did not lead to perceptible crosslinking of αS, in contrast to the $Ru(bpy)_3^{2+}/S_2O_8^{2-}$/light system. A similar photocrosslinking behavior has been observed for the amyloid β-protein (Aβ), with which the formation of LMWO was only also obtained by combination of the $Ru(bpy)_3^{2+}$, APS, and light [38].

Western blots of the protein reaction mixture employing specific monoclonal antibodies against αS (syn211) and diTyr (1C3) (Fig. 1d) indicated that a positive specific diTyr antibody reaction was observed only for the oligomeric species, i.e., $(\alpha S)_2 \ldots (\alpha S)_{n>4}$, and not for the monomeric αS of both controls (either irradiated or dark) of protein solutions irradiated in the presence of $Ru(bpy)_3^{2+}/S_2O_8^{2-}$. This result confirmed the involvement of diTyr groups as covalent bridges between protein molecules arising as a consequence of the reaction of photogenerated side-chain tyrosyl radical (αS–$Tyr^{\bullet}$) in accordance with Eqs. (3)–(7). It is noteworthy that no *intramolecular* diTyr formation in the remaining monomeric αS was detectable by immunochemistry.

The UV–vis absorption and emission spectral changes produced during the photocrosslinking reaction are shown in Fig. 2a–f. The absorption spectra of 104 μM protein solution (gray line) and of the photosensitizer mixture $Ru(bpy)_3^{2+}/S_2O_8^{2-}$ (dashed black line) at the same concentration used in the reaction are shown in Fig. 2a. Before irradiation of the $Ru(bpy)_3^{2+}$ complex with blue light, the initial spectrum of the reaction mixture was equivalent to the sum of the individual spectra of the protein and of the photosensitizer, indicating the absence of apparent specific interactions, e.g., charge-transfer type, between the αS and the metal complex. After illumination of the solution, a continuous increment in the absorbance at < 400 nm was observed, while the typical MLCT band of the $Ru(bpy)_3^{2+}$ complex above 400 nm remained unaltered, demonstrating the absence of sensitizer degradation. We conclude that a new chromophoric species was produced, leading to the changes observed in the UV region. Fig. 2b shows the time evolution of the difference spectrum ($\Delta A_\lambda = A_t - A_0$), confirming the formation of new absorbing species with maxima at 237 and 294 nm and a shoulder at 320 nm. These spectral features are closer to those observed for the diTyr chromophore at neutral pH [37], and consistent with the Western blots results obtained with the specific monoclonal antibody 1C3 that confirmed the formation of diTyr (Fig. 1d).

Inasmuch as WT αS does not contain Trp residues, and in view of the similarity of the absorbance changes observed after photosensitization with the spectrum of the isolated diTyr chromophore at a similar pH, the total concentration of diTyr could be estimated using the absorbance increment at 315 nm and the value $\varepsilon = 5 \times 10^3\ M^{-1}\ cm^{-1}$ at pH 7.5 [45] (Fig. 2c). After 500 s of the photocrosslinking reaction, the concentration of dyTyr reached ~28 μM, representing ~50% of the total tyrosine content. The ensuing plateau indicated that the formation of diTyr was limited to this extent of reaction, presumably due to stereochemical factors.

The formation of diTyr during the photo-initiated crosslinking of αS was also assessed by fluorescence spectroscopy (Fig. 3d, excitation at 275 nm). Prior to irradiation, only the typical Tyr emission band with maximum at 305 nm was observed. After selective irradiation of $Ru(bpy)_3^{2+}$ with blue light (450 nm) in the presence of $S_2O_8^{2-}$, the Tyr emission band was reduced, with the simultaneous appearance of a new band with a maximum at 405 nm, typical of the diTyr fluorophore [37]. The assignment of the fluorescence to diTyr was confirmed by the emission and excitation spectra, obtained by excitation at 320 nm and emission at 405 nm, respectively (Fig. 3e), which corresponded with published data obtained at a similar pH [37]. The isoemissive point at 338 nm observed on excitation at 275 nm confirmed that the Tyr degradation was kinetically linked to the formation of diTyr. The ratio of the fluorescence intensity at both maxima, e.g., $F_{405}/F_{305}$, can be considered to be proportional to the concentration ratio of diTyr and Tyr, and thus serves as a measurement of the degree of conversion of the photocrosslinking reaction. This ratio increased linearly with irradiation time (Fig. 2f), suggesting that the efficiency of the photocrosslinking of αS was proportional to the steady-state concentration of the photogenerated side-chain tyrosyl radical intermediate (see below). Finally, the new diTyr emission band showed a mean steady-state anisotropy value $\langle r \rangle \approx 0.17$ at all irradiation times (Fig. 2f), indicating that the product diTyr had similar rotational diffusion properties in all oligomeric species.

The mixture of crosslinked peptides was digested with trypsin and analyzed by mass spectrometry (MS). The resulting spectra were compared to those corresponding to the monomeric αS, based on high accuracy MS and MS/MS fragment ions shown in

Fig. S1 of the ESM. Three different peaks at $m/z$ 950.5, 1309.6, and 1237.6 were identified as αS crosslinked peptides and confirmed to be: (a) a homodimer peptide involving N-terminus residues of αS, including Y39, i.e., $(E35\text{-}K43)_2$; (b) a heterodimer peptide involving the previous smaller N-terminus peptide and a larger C-terminus peptide that includes the others three Tyr residues of αS (Y125, Y133, and Y136), i.e., (N103-A140) – (E35-K43), and (c) a trimer peptide formed by the combination of two peptides of the N-terminus with the larger C-terminus peptide, i.e., (N103-A140) – 2 × (E35-K43). Furthermore, the mass spectra analysis

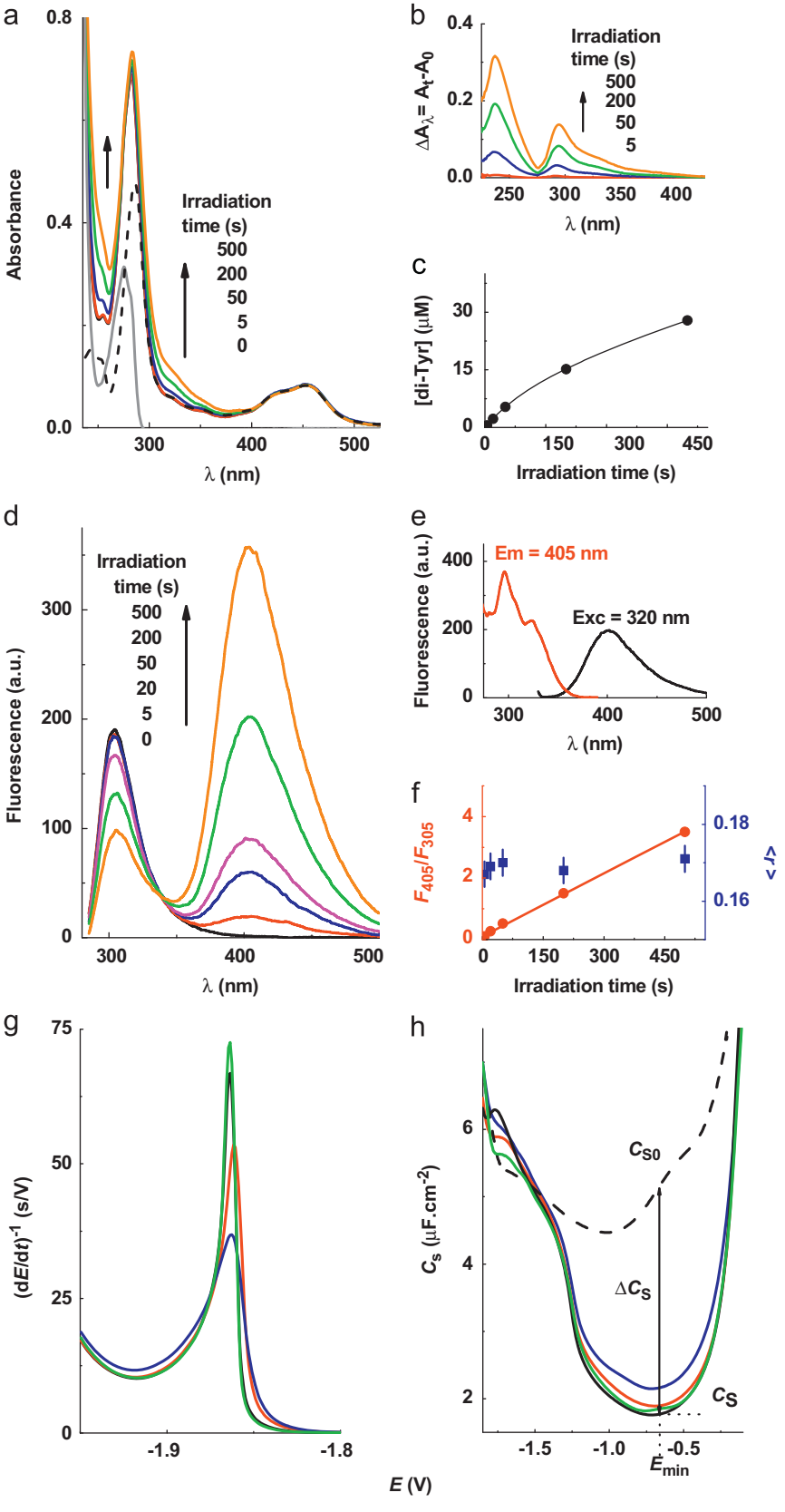

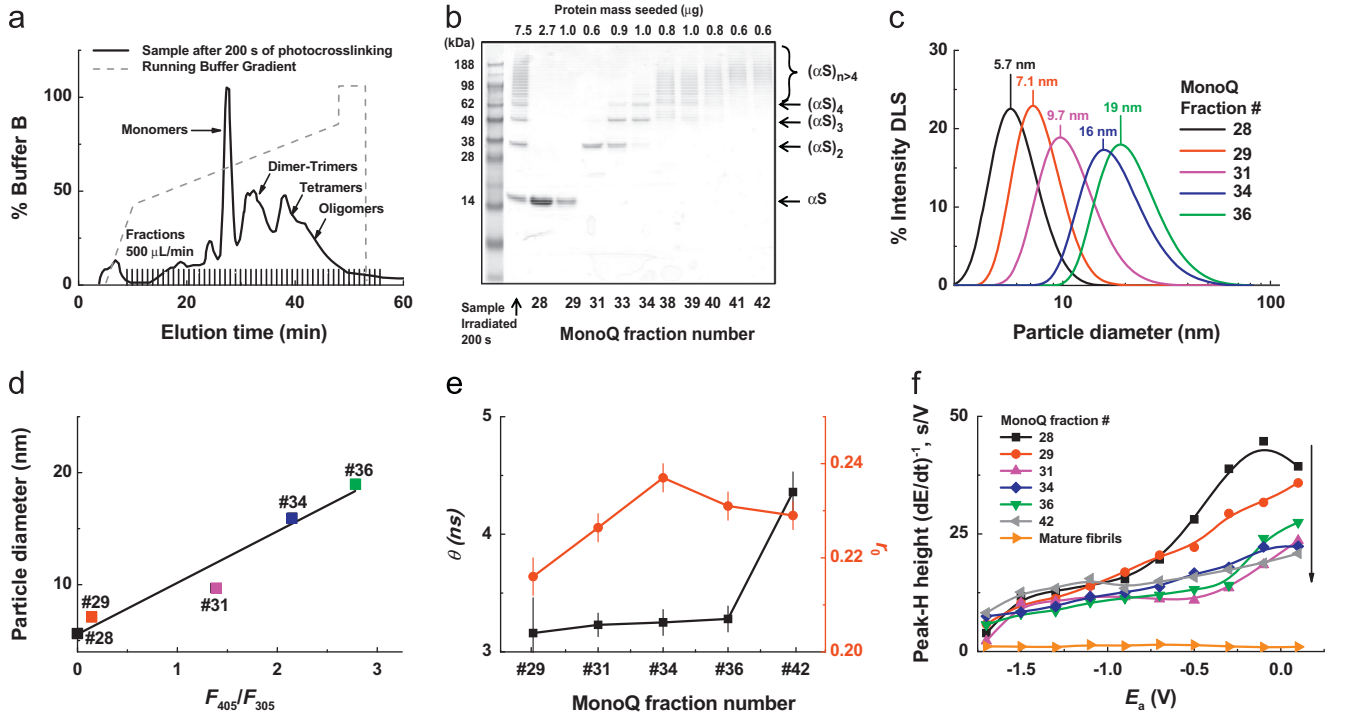


**Fig. 3.** Characterization of oligomeric αS species. (a) Anion-exchange chromatograph of solutions of αS photolyzed with $Ru(bpy)_3^{2+}/S_2O_8^{2-}$ for 200 s. The vertical lines on the elution time axis represents the number of fractions collected after separation with a MonoQ 4.6/100 PE anion-exchange column (see Materials and methods). (b) SDS-PAGE of the reaction mixture after 200 s of photolysis, together with selected fractions collected after separation and purification. (c) Dynamic light scattering (DLS) for particle size estimation of selected fractions of purified αS oligomers. (d) Relationship between particle diameter determined by DLS and diTyr to tyrosine fluorescence intensity ratio $F_{405}/F_{305}$ of selected fractions (numbered) obtained by anion-exchange chromatography. (e) Rotational correlation time $\theta$ (black squares) and initial anisotropy $r_0$ (red circles), and (f) dependence of CPS peak H heights on accumulation potential $E_a$ for several purified fractions.

did not show evidence of Tyr reaction with amino acid residues of the hydrophobic central NAC region, nor of crosslinking reactions involving either Met or His residues. A minor contribution of oxidized Met residues was detected, but these modifications were also present in the untreated control monomer, probably arising during handling, triyptic digestion, and preparation of the protein for MS analysis. Putative Tyr-Lys crosslinking bridges could be theoretically possible [29], but they were also not in evidence in the high accuracy peptide MS/MS analysis. It can be concluded that the formation of the covalent oligomers by photoinduced crosslinking of αS occurs via di-Tyr bridges.

The course of the photocrosslinking reaction of αS was also monitored by chronopotentiometric stripping (CPS) analysis (producing electrocatalytic peak H) and phase-sensitive a.c. voltammetry (phase angle 90°) at the hanging mercury drop electrode, methods we used previously to study changes in the interfacial properties of αS during the course of aggregation [46]. CPS peak H corresponds to the catalytic hydrogen evolution reaction [47], and differs from previously described voltammetric responses of proteins by (a) different manner of electrode polarization; (b) its ability to detect proteins down to nanomolar and subnanomolar concentrations; and (c) high sensitivity to changes in protein structures. The specific differential capacity ($C_s$) of the electrode double layer is a sensitive indicator of adsorption at the electrodes [46,48]. In proteins absorbed at nearly neutral pH values, only accessible Lys, Arg and Cys residues are predominantly involved in catalytic hydrogen evolution reaction [47,49,50]. Since αS lacks Arg or Cys, only the 15 Lys residues per protein molecule can give rise to the electrocatalytic activity. Fig. 2g shows the peak H of 300 nM αS adsorbed at HMDE after several photocrosslinking conditions. Nonirradiated monomeric αS in the absence or presence of the photosensitizing mixture $Ru(bpy)_3^{2+}/S_2O_8^{2-}$ produced almost the same well-developed peak H. Furthermore, the decreases of $\Delta C_s$ over a wide potential range of about −0.1 to −1.2 V indicated that the αS conformation and adsorbability in this potential range were not significantly affected by either $Ru(bpy)_3^{2+}$ or $S_2O_8^{2-}$ (Fig. 2h). In contrast, after irradiation of the photosensitizing mixture, the height of peak H decreased nearly by ~20 and 45% after irradiation for 20 and 200 s, respectively. Furthermore, the $\Delta C_s$ value decreased by about

**Fig. 2.** Spectroscopic and electrochemical changes produced during photoinduced crosslinking of αS: (a) UV–vis spectral changes (optical path 5 mm) of the photolyzed solution of αS (104 µM) in 25 mM Na-$PO_4$, pH 7.4 buffer with 15 µM $Ru(bpy)_3^{2+}$/300 µM $S_2O_8^{2-}$ exposed to continuous light (450 nm, 2.2 mW/cm$^2$). The individual spectra of 104 µM αS (grey solid line) and 15 µM $Ru(bpy)_3^{2+}$ (black dashed line) are also presented to confirm the spectral sum. (b) Differential spectral changes obtained by subtraction of the initial absorbance spectrum of the reaction mixture ($\Delta A_\lambda = A_{\lambda,t} - A_{\lambda,0}$). (c) Kinetic profile of the diTyr chromophore concentration calculated with $\varepsilon_{315} = 5 \times 10^3$ $M^{-1}$ $cm^{-1}$ [45]. (d) Fluorescence emission spectral changes of the irradiated solutions; excitation at 275 nm. The numbers on the spectra indicate the cumulative irradiation times in s. (e) Excitation (red line) and emission (black line) spectra of the reaction mixture irradiated after 500 s with blue light, monitored with emission at 405 nm and excitation at 320 nm, respectively. (f) Variation of the fluorescence intensity ratio between 405 and 305 nm ($F_{405}/F_{305}$) of the reaction mixture (red circle symbols) and of the diTyr fluorescence anisotropy (square blue symbols) obtained by excitation at 275 and 320 nm, respectively, as a function of the irradiation time. (g) Peak H; and (h) C–E curves corresponding to αS without sensitizer ions and light exposure (green solid line); no-irradiated αS in presence of $Ru(bpy)_3^{2+}/S_2O_8^{2-}$ (black solid line), and irradiated αS with $Ru(bpy)_3^{2+}/S_2O_8^{2-}$ for 20 s (red solid line) and 200 s (blue solid line), respectively. αS was adsorbed at HMDE for accumulation time ($t_A$) 60 s at accumulation potential $E_A - 0.1$ V, followed by chronopotentiogram or C–E curve recording. The background electrolyte contribution in C–E plot is also indicated with the dashed black line. $C_s$ is the differential capacity of the αS-modified hanging mercury drop electrode (HMDE) at the given potential; $C_{s0}$, is the value of bare HMDE in the background electrolyte; $\Delta C_s = C_s - C_{s0}$. $E_{min}$ indicates the potential at which $C_s$ reaches its minimum value. (For interpretation of the references to color in this figure legend, the reader is referred to the web version of this article.)

4 and 15% after irradiation for 20 and 200 s, respectively, compared to the nonirradiated sample. These changes in peak H and $\Delta C_s$ can be related to the decrease in accessibility of electroactive Lys residues resulting from oligomer formation [48].

### αS oligomer purification and characterization

The oligomer mixture of αS obtained after 200 s of photolysis was purified and separated by anion-exchange chromatography (Fig. 3a). As expected, the elution times of the chromatographic peaks were proportional to the mass of the oligomeric species. After separation, the collected fractions were reanalyzed by SDS-PAGE (Fig. 3b). The electrophoretic analysis indicated that monomeric protein was present in fractions 28 and 29, whereas fractions 31 and 34 were composed mainly of dimers $(\alpha S)_2$ and trimers $(\alpha S)_3$. Tetramers $(\alpha S)_4$ were the main component of the fraction 36 (not shown in this gel). The rest of the fractions contained mixtures of higher order oligomers $(\alpha S)_{n>4}$, which were not separated by the chromatographic procedure. All fractions with protein with mass >28 kDa showed the characteristic absorption and emission bands of diTyr chromophore (Fig. S2 of ESM), confirming the results from Western blots using the antibody 1C3 (Fig. 1d). Despite the lack of a spot for monomeric αS in the anti-diTyr Western blot, the monomeric fraction 29 collected at the tail of the monomer chromatographic peak showed a very weak fluorescence signal attributable to diTyr (Fig. S2).

Dynamic light scattering measurements confirmed a continuous increment of particle size with the fraction number of purified oligomer (Fig. 3c). In fact, the particle diameter of fractions 31, 34, and 36 increased 2- to 4-fold compared to monomeric αS (28). The progressive size increment was in good agreement with the molecular mass characterization of the oligomer species of the same fractions in the SDS-PAGE (Fig. 1a). In addition, the observed particle diameter of the collected fractions was nearly linear with the fluorescence intensity ratio $F_{405}/F_{305}$, reflecting the proportionality between the increment in molecular size and the content of diTyr bridges in the oligomeric species (Fig. 3d).

The fluorescence decay of the diTyr bridges in the different fractions was monitored at 405 nm. The decay showed a biexponential behavior with lifetimes of $\sim 2.4 \pm 0.5$ and $4.8 \pm 0.3$ ns and fractional contributions of $0.27 \pm 0.03$ and $0.73 \pm 0.05$, respectively. These results indicate that no significant changes in the molecular microenvironment sensed by the diTyr bridge accompanied the increment in oligomer size. The analysis of the fluorescence anisotropy decay yielded similar conclusions. The rotational correlation time $\theta$ obtained by monoexponential fitting of the anisotropy decay according to the isotropic rotational model $r(t)=r_0 e^{-t/\theta}$ was $3.2 \pm 0.1$ ns for the collected fractions, corresponding to LMWO (fractions 31–36, dimers to tetramers), and increased to $4.2 \pm 0.2$ ns for HMWO (42, $(\alpha S)_{n>4}$), while the initial anisotropy $r_0$ increased slightly from 0.22 for fraction 31 to 0.23 for fraction 42 (Fig. 3e). These results were consistent with the size increment of the oligomeric species.

The chronopotentiometric stripping analysis of the different collected fractions indicated that the relatively high peak H of fraction 28 (wild-type monomer) obtained at $E_A = -0.1$ V strongly decreased with shifting $E_A$ to $\sim -1$ V (Fig. 3f). Between $E_A \sim -1$ and $-1.5$ V the peak heights decreased only slightly with shifting of $E_A$ to negative values. Peak H of fraction 29 obtained at $E_A$ $-0.1$ V was ~20% smaller (compared to that of fraction 28) and displayed a similar dependence on $E_A$ as fraction 28, suggesting a decrease in the number of accessible electroactive Lys residues. Peak H heights of the oligomers (fractions 31, 32, 34, 36, and 42) obtained at $E_A - 0.1$ V were ~50% smaller than that of the monomer and showed a much smaller decrease on shifting $E_A$ to negative potentials. Similarly the *C–E* curves of oligomers displayed a strong decrease of the capacity of the electrode double layer between $-0.1$ and $-1$ V as compared to the monomer (Fig. S3 of ESM), suggesting weaker adsorption of large αS oligomers in this potential region. The electrochemical response of mature fibrils obtained by long-term incubation of 100 μM wild-type αS at 37 °C was also evaluated. In this case, the signal of peak H was absent as a result of the lack of adsorbability of the larger fibrils.

### Effect of covalent oligomerization on the noncovalent aggregation of αS and cytotoxicity on SH-SY5Y cells

The effect of covalent oligomers on the noncovalent aggregation kinetics of wild-type αS was evaluated in 30 mM Tris–HCl buffer, pH 7.3, by monitoring both the temporal evolution of the second-order scattering intensity at 680 nm ($I_{680}$) and the fluorescence intensity of ThioT at 480 nm ($F_{480}$) at 37 °C [24]. In all cases, the photosensitizing ions $Ru(bpy)_3^{2+}/S_2O_8^{2-}$ were first removed by ultrafiltration. Fig. 4a shows the time course of $I_{680}$

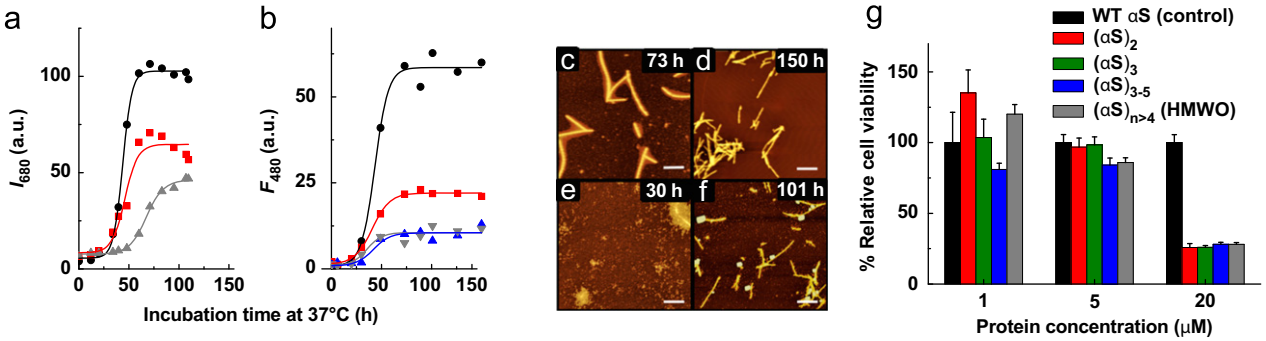


**Fig. 4.** Effect of covalent crosslinking of αS on its aggregation and on the viability of differentiated SH-SY5Y cells at 37 °C. (a) Time course of the second-order scattering (with $\lambda_{ex}=340$ nm) during the aggregation of αS as a function of extent of photocrosslinking reaction: 100 μM αS in 30 mM Tris–HCl, pH 7.5 (control, black circles) and of the same solution after 20 s (red squares) and 200 s (up gray triangles) of blue-light irradiation in the presence of $Ru(bpy)_3^{2+}/S_2O_8^{2-}$. (b) ThioT assay for the aggregation of 100 μM αS in 30 mM Tris–HCl (pH 7.5) at 37 °C (control, black circles) with the addition of 20 μM of different purified covalent oligomeric species: dimers ($(\alpha S)_2$, red squares); tetramers ($(\alpha S)_4$, up blue triangles); and HMWO ($(\alpha S)_{n>4}$, down gray triangles). The solid lines represent the data fitting curve (Eq. (8)), for which the resulting fitting parameters are presented in Table 1. (c–f) AFM imaging of aggregation of WT αS alone and in presence of covalent dimers $(\alpha S)_2$. The images correspond to the samples featured in panel b: 100 μM αS WT after 73 h (c) and 150 h (d) of incubation; and 100 μM αS + 20 μM covalent dimers after 30 h (e) and 101 h (f) of incubation, respectively. Scale bar: 500 nm. (g) Differentiated SH-SY5Y cells were incubated 40–44 h with 1, 5, and 20 μM monomeric or crosslinked fractions of αS in DMEM + Hepes serum-free media. The cytotoxic effect of the different fractions of crosslinked oligomers was assayed with the WST-1 Cell Proliferation Reagent (Roche). Significant differences were determined by the Student *t* test ($^*P < 0.05$).(For interpretation of the references to color in this figure legend, the reader is referred to the web version of this article.)

of 100 μM αS solutions before irradiation (control), and after irradiation for 20 and 200 s. According to the densitometry analysis of the SDS-PAGE (Fig. 1b), the sample composition after 20 s of irradiation was ~89% monomer αS and 11% dimeric species $(\alpha S)_2$, whereas in the sample irradiated for 200 s the monomer consumption was close to 60% with the formation of a complex mixture of covalent oligomers (dimers, trimers,…, HMWO). In a second experimental protocol, a fixed concentration of the different purified covalent oligomeric species was added to monomeric protein to yield a final mixture of 20 μM oligomers and 100 μM wild-type αS. Fig. 4b shows the aggregation kinetics monitored by ThioT fluorescence by sampling during the time course of incubation. The scattering and fluorescence curves were fitted according to Eq. (8) (Table 1).

In the case of the oligomer formation in situ, a progressive decrease of the apparent growth rate constant $k_{app}$ and a parallel increase in $t_{1/2}$ were observed. These effects can be attributed to the effective reduction of the initial αS concentration, $[\alpha S]_0$, i.e., from initial 100 μM to 90 and 60 μM after irradiation for 20 and 200 s, respectively, since the second-order rate constant for incorporation of the monomer into the growing amyloid fibrils $k_{agg}$ remained almost constant (Table 1) [51].

A similar effect was observed on addition of 20 μM of purified covalent oligomers to 100 μM αS, indicating that these species do not modify the rate of amyloid formation. However, the covalent oligomeric species strongly reduced the signal change (i.e., $\Delta Y$ evaluated as $\Delta I_{680}$ or $\Delta F_{480}$ between the final and the initial times of the experiment), which is a measure of the final yield of amyloid fibrils. The relative conversion $\beta\,(=\Delta Y_{OLIG}/\Delta Y_{WT})$ showed a correlation with the sample composition, such that the reduction in the amyloid yield increased from dimers $(\alpha S)_2$ to tetramers $(\alpha S)_4$, with HMWO $(\alpha S)_{n>4}$ exhibiting an effect similar to that of tetramers (Table 1).

In view of the inhibitory effects of covalent oligomeric species on the noncovalent aggregation of bulk WT αS, AFM imaging of the resulting products was performed (Fig. 4c–f). In a parallel study, this technique has revealed a family of distinct supramolecular intermediates in the aggregation of αS [25].

The aggregation imaging of WT αS showed the progression from "fuzzy fibers" [25] and small spherical noncovalent oligomeric intermediate species after 73 h (Fig. 4c), to the complete formation of mature amyloid fibers at the end of the aggregation process (150 h, Fig. 4d). In contrast, the presence of covalent dimers $(\alpha S)_2$ produced a larger number of small spherical intermediates at the onset of fibril formation at 30 h (Fig. 4e), which persisted after 101 h of incubation, at which time a smaller yield of fibrils was also observed (Fig. 4f). These results are consistent with the lower relative yield of β-sheet amyloid formation ($\beta=0.34$, Table 1). An additional feature of the final fibrils formed in the presence of $(\alpha S)_2$ was an irregular and branched structure.

The biological properties of photocrosslinked oligomeric species of αS were assessed by determinations of differential toxicity on neuronal-like cells. Purified fractions were prepared, quantified by SDS-PAGE (Fig. S4 and Table S1 of ESM), and applied extracellularly to differentiated SH-SY5Y cells in a test of cytotoxicity. After differentiation, the cells were incubated for 40–44 h in serum-free media supplemented with 1, 5, and 20 μM protein of monomeric wild-type αS (control) or the following oligomeric fractions composed mainly of dimers $(\alpha S)_2$, trimers $(\alpha S)_3$, a mixture of $(\alpha S)_3$, $(\alpha S)_4$, and $(\alpha S)_5$), and >95% HMWO$(\alpha S)_{n>4}$, corresponding to the collected fractions III, IV, VII, and VIII of the gel in Fig. S4. The metabolic rate was measured employing the WST-1 Cell Proliferation Reagent (Roche Applied Science) and the cytotoxic effect was estimated as a relative viability by normalization with values obtained with monomeric αS (Fig. 4g). No significant effects were observed on addition of ≤5 μM of either monomeric or covalent oligomeric αS species, but a distinct cytotoxicity was evident at 20 μM concentrations of all the oligomeric species. WT αS also showed a small dose-dependent effect compared to cells incubated with protein-free media (Fig. S5), a result that we attribute to the formation of noncovalent cytotoxic oligomeric species of WT αS in differentiated SH-SY5Y cells.

## Discussion

### *Mechanistic and kinetic analysis of the formation of covalent oligomers of αS*

The results presented above are consistent with the progressive formation of covalent oligomeric species of αS induced by photosensitization with the $Ru(bpy)_3^{2+}/S_2O_8^{2-}$/light system. In accordance with the photosensitized crosslinking model proposed ((Eqs. (1)–(7)), the formation of diTyr groups mediated by tyrosyl radicals was unequivocally demonstrated in this study by immune detection analysis (Fig. 1d), the characteristic absorption and fluorescence spectra of diTyr after irradiation (Fig. 2a–e), and the MS analysis of the fragmentation profile of each crosslinked peptide with b- and y-type peptides (Fig. S1), indicating that potentially all Tyr residues can react to form crosslinked αS. In the peroxidation of αS with cytochrome $c+H_2O_2$, Ruf et al. [15] reported that the relative reactivity of the Tyr residues in forming diTyr bonds was Y39 < Y125 < Y133, Y136. Furthermore, Souza et al. [12] showed that exposure to peroxynitrite also led to the formation of SDS and heat-stable αS oligomers resulting from diTyr crosslinking, mainly involving C-terminal Tyr residues. However, the present results demonstrate that despite its relative lower reactivity, the Y39 residue is involved in tyrosyl radical-induced covalent oligomerization of αS, since the shorter crosslinked peptide $(E35\text{-}K43)_2$ at $m/z$ 950.5 (Fig. S1a) is undoubtedly formed by a Y39-Y39 crosslink. Y39 must also be involved in the crosslinked hetero dimer peptide at $m/z$ 1309.6 (Fig. S1b) and in the crosslinked trimer peptide at $m/z$ 1237.6 (Fig. S1c), arising by reaction with any of the C-terminal Tyr residues (e.g., Y125, Y133,

**Table 1**
Aggregation parameters of WT α-synuclein, incubated at 37 °C mixed with different proportions of covalent oligomeric species of the protein obtained by photoinduced crosslinking using $Ru(bpy)_3^{2+}/S_2O_8^{2-}$ as sensitizing ions. Analysis according to Eq. (8).

| | Sample | $\Delta Y$ (a.u.) | $k_{app}$ ($h^{-1}$) | $t_{1/2}$ (h) | $R^2$ | $k_{agg}/10^3$ ($M^{-1}$ $h^{-1}$) | $\beta=(\Delta Y_{OLIG}/\Delta Y_{WT})$ |
|---|---|---|---|---|---|---|---|
| second-order light scattering assay | 100 μM αS (control 1) | 97 ± 2 | 0.22 ± 0.02 | 44 ± 5 | 0.997 | 2.2 ± 0.1 | 1.00 ± 0.01 |
| | 89% αS + 11% $(\alpha S)_2$ | 56 ± 5 | 0.16 ± 0.05 | 46 ± 3 | 0.943 | 1.8 ± 0.2 | 0.58 ± 0.06 |
| | 60% αS + 40% $(\alpha S)_n$ | 38 ± 2 | 0.12 ± 0.01 | 67 ± 1 | 0.993 | 2.0 ± 0.1 | 0.39 ± 0.02 |
| Thio-T fluorescence assay | 100 μM αS (control 2) | 58 ± 2 | 0.15 ± 0.03 | 43 ± 2 | 0.988 | 1.5 ± 0.3 | 1.00 ± 0.03 |
| | 100 μM αS + 20 μM $(\alpha S)_2$ | 20 ± 1 | 0.11 ± 0.02 | 41 ± 1 | 0.995 | 1.1 ± 0.2 | 0.34 ± 0.01 |
| | 100 μM αS + 20 μM $(\alpha S)_4$ | 10 ± 1 | 0.12 ± 0.04 | 42 ± 2 | 0.981 | 1.2 ± 0.4 | 0.17 ± 0.02 |
| | 100 μM αS + 20 μM $(\alpha S)_{n>4}$ | 10 ± 1 | 0.13 ± 0.08 | 36 ± 6 | 0.876 | 1.3 ± 0.1 | 0.17 ± 0.02 |

or Y136). These results highlight the importance of Y39 in the formation of trimers and higher order oligomers, as suggested previously by Ruf et al. [15].

According to mass spectrometry analysis, only diTyr crosslinked peptides were detected, indicating the prevalence of the reaction between side-chain tyrosyl radicals and/or with another Tyr residue instead of with other amino acid residues. This assumption is supported by the densitometry analysis of the monomeric band (~14.4 kDa) of the SDS-PAGE of Fig. 1b. After 500 s of photocrosslinking the final conversion of monomeric αS to oligomeric species was ~56%, representing ~58 μM crosslinked monomeric αS, almost twice the concentration (~28 μM) of total diTyr formed, as calculated from the differential absorption changes at 315 nm.

The SDS-PAGE characterization of the ion-exchange chromatography-purified fractions 31, 34, and 36 indicated that they were mainly composed of $(\alpha S)_2$, $(\alpha S)_3$, and $(\alpha S)_4$, respectively (Fig. 3b). The particle diameter determined by DLS (Fig. 3c) of these fractions was only ~7–17% smaller than expected assuming a stepwise addition of monomeric αS (i.e., 5.7 nm × $n_{2-4}$). Furthermore, the covalent oligomerization of αS was proportional to the number of diTyr bonds formed (Fig. 3d). However, only fraction 29 showed a similar molecular mass as WT αS (fraction 28), albeit with a larger 1.4 nm particle diameter and a very weak diTyr fluorescence signal (Fig. 3b–d). Furthermore, the structural modification of this monomeric fraction 29 was also confirmed by chronopotentiometric stripping experiments, since the decreases of the peak H high relative to WT αS (i.e., fraction 28 in Fig. 3f) could be the result of a diminished number of accessible electroactive Lys residues due to conformational changes. Therefore, despite the lack of anti-diTyr reactivity in the Western blot band for monomeric αS (Fig. 1c) these results, together with the spectroscopic behavior noted before, suggest that a very small fraction of monomeric αS could be photocrosslinked by intramolecular Tyr–Tyr bonds.

For the covalent oligomers of αS (e.g., fractions 31, 32, 34, 36, and 42) the peak H height obtained at $E_A - 0.1$ V was ~50% smaller than that of the monomer and showed a much smaller decrease and shifting of $E_A$ to negative potentials. Similarly the *C–E* curves of the oligomers displayed a strong decrease of the capacity of the electrode double layer between −0.1 and −1 V as compared to the monomer (Fig. S3 of EMS), suggesting weaker adsorption at the electrode for the HMWO of αS in this potential region, probably influenced by changes in the size and shape of the oligomers affecting their adsorption properties and the accessibility of the electroactive Lys residues. Interestingly, the electrochemical response for these soluble covalent oligomers of αS followed the trend of that obtained in the course of the WT protein aggregation (under the given conditions), which results in the absence of peak H for mature fibrils obtained after long-term incubation of 100 μM wild-type αS at 37 °C (Fig. 3f).

According to the all experimental evidence, the photoinduced crosslinking mechanism of αS can be regarded as a branched process, predominantly involving intermolecular reaction steps mediated by the side-chain tyrosyl radical of αS ($\alpha S^\bullet$) as the main intermediate (Scheme 1). For simplicity, terminating reactions between accumulated monomeric and/or oligomeric radical species are omitted. The reaction scheme explains approximately the formation and consumption of LMWO ($(\alpha S)_{n\le 4}$) at protein concentrations high enough to ensure a nearly constant photostationary concentration of the precursor monomeric radical $\alpha S^\bullet$. In agreement with Eqs. (1)–(4), the irradiation of $Ru(bpy)_3^{2+}$ in the presence of $S_2O_8^{2-}$ leads to the formation of $\alpha S^\bullet$, which at the beginning of the process can be expected to be completely scavenged by the excess of unmodified monomeric αS to form dimers $(\alpha S)_2$. After accumulation of $(\alpha S)_2$, the reaction with extra $\alpha S^\bullet$ leads to the formation of trimers $(\alpha S)_3$, but also possible is the generation of tetramers $(\alpha S)_4$, by reaction with new radical intermediate $(\alpha S)_2^\bullet$ photogenerated by the $Ru(bpy)_3^{2+}/S_2O_8^{2-}$ system. Thus, the progressive formation of radical intermediate species of high MW, i.e., $(\alpha S)_n^\bullet$, results in the slower consumption rate of the unmodified monomer due to the decreased diffusion rate of the oligomeric species as well as the reduced monomer concentration. According to the data, the intraprotein formation of diTyr appears to be a minor reaction pathway, probably reflecting the random conformation of the protein and the relative orientation of the Tyr residues of the monomeric αS in solution.

### *Role of covalent oligomers of αS formed by oxidative stress in PD etiology*

In order to establish the relevance of covalent oligomers formed in response to oxidative stress, we analyzed the capacity of purified fractions of αS oligomeric species to modify the natural tendency to form amyloid fibrils, and to evaluate the toxicity they exerted on differentiated neuronal-like SH-SY5Y cells. As shown in Fig. 4a–b and Table 1, the formation of diTyr covalent oligomers decreased the yield of amyloid fibril formation during in vitro αS aggregation. The AFM images of Fig. 4c–f confirmed that photocrosslinked oligomers are able to short-circuit the β-sheet fibril amyloid path in favor of the formation of smaller, spherical and round-like intermediates. These results are in accordance with the observations of Ruf et al. [15] on the aggregation of peroxidated αS, indicating that covalent oligomeric crosslinked species

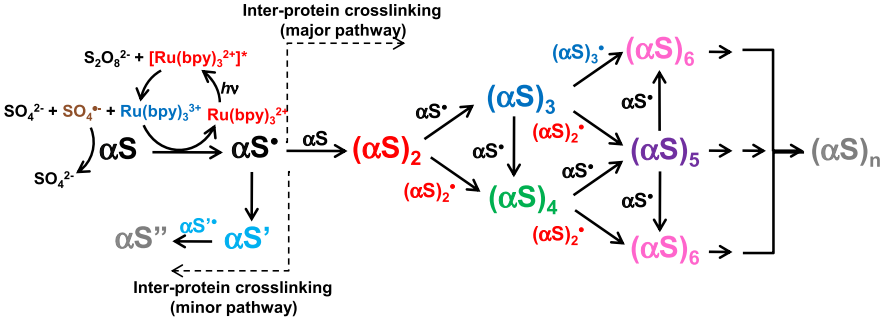


**Scheme 1.** . Proposed reaction scheme for photo-initiated tyrosyl radical ($\alpha S^\bullet$) mechanism of photocrosslinking of αS. The formation of several covalent oligomeric species of αS is mainly controlled by the photo-stationary concentration of $\alpha S^\bullet$ initiated by the system $Ru(bpy)_3^{2+}$/ammonium persulfate. The accumulation of low molecular weight oligomers LMWO $(\alpha S)_{n=2-4}$ increases the probability of intermediate radical species with higher molecular weight HMWO, e.g., $(\alpha S)_{n=2-4}^\bullet$. For simplicity, terminating reactions between accumulated monomeric and/or oligomeric radical species have been omitted.

of αS constitute a trap altering the overall mechanism such that final amyloid fibril formation is inhibited or reduced.

The exposure of differentiated SH-SY5Y cells to the covalent species at 20 μM led to significant cytotoxicity (Fig. 4g). The effect was the same regardless of the stoichiometry of the oligomers, suggesting that in the in vivo radical oxidative stress scenario, the accumulation of simple covalent dimeric species of αS may suffice for inducing cellular damage. These results are consistent with the current concept that oligomeric intermediate species, rather than mature amyloid fibrils, constitute the main culprits in the pathogenesis of PD [52,53]. It is possible that the radical-mediated covalent oligomerization of αS described above may promote the appearance of more toxic species and/or prevent their neutralization into mature amyloid fibrils, explaining why oxidative stress has always been closely correlated with PD and similar pathologies [9]. We propose that this type of intermediate appears during the initial steps of αS pathology, affecting the neutralization or disposal of toxic species into mature amyloid aggregates and exacerbating their toxicity. It has been reported recently that SH-SY5Y cells overexpressing αS and subjected to stress conditions release damaged forms of the protein via nonclassical exocytosis [54]. Furthermore, selective glycolipids seem to function as specific receptors in microglia that promote αS internalization [55]. Therefore, the toxicity observed for extracellularly added modified αS is consistent with the proposal that the pathological state of affected/dying neurons can be propagated to neighboring cells by release of toxic/oxidized cytoplasmic components [56], initiating a chain reaction, possibly with characteristics of a prion-like process [57] and/or an inflammatory response [58], including the induction of aggregates in neighboring cells [56,59]. We observed direct toxicity of oxidized/oligomeric species of αS on target cells. This result is consistent with the notion that the high concentrations of compounds promoting radical-mediated oxidation of proteins, such as dopamine or polyunsaturated lipids in dopaminergic neurons, may account for the role of oxidative stress as a major trigger of a(the) initial processes leading to the development of PD.

## Conclusions

Photosensitized crosslinking is a very suitable method for the controlled formation of defined covalent linked oligomeric species of αS by side-chain tyrosyl radicals generated by the metal coordination complex $Ru(bpy)_3^{2+}$ in the presence of $S_2O_8^{2-}$. The role of Tyr–Tyr as covalent crosslinkers was demonstrated by SDS-PAGE/Western blot, spectroscopic, mass spectrometry, and electrochemical methods. The relationship between these covalent intermediates in the aggregation and toxicity of αS has also been elucidated. In accordance with similar results obtained for amyloid β [38,39], we propose that photoinduced generation of side-chain tyrosyl radicals mimics radical-induced oxidative stress conditions experienced by cells and can be generalized to other model systems of toxic proteins involved in different neurodegenerative diseases.

## Acknowledgments

The author Elizabeth A. Jares-Erijman passed away during the final part of this study. The surviving authors mourn this great loss and dedicate this publication to her memory in acknowledgment of her support, inspiration, and leadership. C.D.B. and L.J.F.L. thank the Alexander von Humboldt Foundation of Germany for Georg Forster fellowships; and J.A.F. to CONICET of Argentina for a Ph.D. fellowship. This work was supported by the Toxic Proteins Project of the Max Planck Society: the Cluster of Excellence 171 of the DFG Center for the Molecular Physiology of the Brain (T.M.J.), FONCyT (PICT06-01090) of Argentina to C.D.B., and a DFG founding (SFB 860) to H.U. This work was also supported by AS CR KJB100040901, M20004090 to V.O.

## Appendix A. Supplementary Material

Supplementary data associated with this article can be found in the online version at http://dx.doi.org/10.1016/j.freeradbiomed.2012.06.035.

## References

[1] Lees, A. J.; Hardy, J.; Revesz, T. Parkinson's disease. *Lancet* **373:**2055–2066; 2009.
[2] Shults, C. W. Lewy bodies. *Proc. Natl. Acad. Sci. USA* **103:**1661–1668; 2006.
[3] Uversky, V. N.; Eliezer, D. Biophysics of Parkinson's disease: structure and aggregation of α-synuclein. *Curr. Protein Pept. Sci.* **10:**483–499; 2009.
[4] Maguire-Zeiss, K. A. α-Synuclein: a therapeutic target for Parkinson's disease? *Pharmacol. Res.* **58:**271–280; 2008.
[5] Bisaglia, M.; Mammi, S.; Bubacco, L. Structural insights on physiological functions and pathological effects of α-synuclein. *FASEB J* **23:**329–340; 2009.
[6] Wang, W.; Perovic, I.; Chittuluru, J.; Kaganovich, A.; Nguyen, L. T. T.; Liao, J. L.; Auclair, J. R.; Johnson, D.; Landeru, A.; Simorellis, A. K.; Ju, S. L.; Cookson, M. R.; Asturias, F. J.; Agar, J. N.; Webb, B. N.; Kang, C. H.; Ringe, D.; Petsko, G. A.; Pochapsky, T. C.; Hoang, Q. Q. A soluble α-synuclein construct forms a dynamic tetramer. *Proc. Natl. Acad. Sci. USA* **108:**17797–17802; 2011.
[7] Bartels, T.; Choi, J. G.; Selkoe, D. J. α-Synuclein occurs physiologically as a helically folded tetramer that resists aggregation. *Nature* **477:**107–U123; 2011.
[8] Spillantini, M. G.; Schmidt, M. L.; Lee, V. M. Y.; Trojanowski, J. Q.; Jakes, R.; Goedert, M. α-synuclein in Lewy bodies. *Nature* **388:**839–840; 1997.
[9] Martinez, A.; Portero-Otin, M.; Pamplona, R.; Ferrer, I. Protein targets of oxidative damage in human neurodegenerative diseases with abnormal protein aggregates. *Brain Pathol.* **20:**281–297; 2010.
[10] Torres-Bugeau, C. M.; Borsarelli, C. D.; Minahk, C. J.; Chehin, R. N. The key role of membranes in amyloid formation from a biophysical perspective. *Curr. Protein Pept. Sci.* **12:**166–180; 2011.
[11] Olteanu, A.; Pielak, G. J. Peroxidative aggregation of α-synuclein requires tyrosines. *Protein Sci.* **13:**2852–2856; 2004.
[12] Souza, J. M.; Giasson, B. I.; Chen, Q. P.; Lee, V. M. Y.; Ischiropoulos, H. Dityrosine cross-linking promotes formation of stable α-synuclein polymers—implication of nitrative and oxidative stress in the pathogenesis of neurodegenerative synucleinopathies. *J. Biol. Chem.* **275:**18344–18349; 2000.
[13] Pennathur, S.; Jackson-Lewis, V.; Przedborski, S.; Heinecke, J. W. Mass spectrometric quantification of 3-nitrotyrosine, ortho-tyrosine, and o,o '-dityrosine in brain tissue of 1-methyl-4-phenyl-1,2,3,6-tetrahydropyridien-treated mice, a model of oxidative stress in Parkinson's disease. *J. Biol. Chem* **274:**34621–34628; 1999.
[14] Krishnan, S.; Chi, E. Y.; Wood, S. J.; Kendrick, B. S.; Li, C.; Garzon-Rodriguez, W.; Wypych, J.; Randolph, T. W.; Narhi, L. O.; Biere, A. L.; Citron, M.; Carpenter, J. F. Oxidative dimer formation is the critical rate-limiting step for Parkinson's disease α-synuclein fibrillogenesis. *Biochemistry* **42:**829–837; 2003.
[15] Ruf, R. A. S.; Lutz, E. A.; Zigoneanu, I. G.; Pielak, G. J. α-Synuclein conformation affects its tyrosine-dependent oxidative aggregation. *Biochemistry* **47:**13604–13609; 2008.
[16] Morris, A. M.; Watzky, M. A.; Finke, R. G. Protein aggregation kinetics, mechanism, and curve-fitting: a review of the literature. *BBA Proteins Proteomics* **1794:**375–397; 2009.
[17] Roberti, M. J.; Morgan, M.; Menendez, G.; Pietrasanta, L. I.; Jovin, T. M.; Jares-Erijman, E. A. Quantum Dots As Ultrasensitive nanoactuators and sensors of amyloid aggregation in live cells. *J. Am. Chem. Soc.* **131:** 8102–8107; 2009.
[18] Lee, C. C.; Nayak, A.; Sethuraman, A.; Belfort, G.; McRae, G. J. A three-stage kinetic model of amyloid fibrillation. *Biophys. J.* **92:**3448–3458; 2007.
[19] Fink, A. L. The aggregation and fibrillation of α-synuclein. *Acc. Chem. Res.* **39:**628-–634; 2006.
[20] Bertoncini, C. W.; Soledad Celej, M. Small molecule fluorescent probes for the detection of amyloid self-assembly in vitro and in vivo. *Curr. Protein Pept. Sci* **12:**206–220; 2011.
[21] LeVine, H. Quantification of beta-sheet amyloid fibril structures with thioflavin T. *Amyloid, Prions, Other Protein Aggregates* :274–284; 1999.
[22] Thirunavukkuarasu, S.; Jares-Erijman, E. A.; Jovin, T. M. Multiparametric fluorescence detection of early stages in the amyloid protein aggregation of pyrene-labeled α-synuclein. *J. Mol. Biol.* **378:**1064–1073; 2008.
[23] Celej, M. S.; Caarls, W.; Demchenko, A. P.; Jovin, T. M. A triple-emission fluorescent probe reveals distinctive amyloid fibrillar polymorphism of wild-

type α-synuclein and its familial Parkinson's disease mutants. *Biochemistry* **48:**7465–7472; 2009.
[24] Yushchenko, D. A.; Fauerbach, J. A.; Thirunavukkuarasu, S.; Jares-Erijman, E. A.; Jovin, T. M. Fluorescent ratiometric MFC probe sensitive to early stages of α-synuclein aggregation. . *Am. Chem. Soc.* **132:**7860–7861; 2010.
[25] Fauerbach, J.A.; Yushchenko, D.A.; Shahmoradian, S.H.; Chiu, W.; Jovin, T.M.; Jares-Erijman, E.A. Supramolecular non-amyloid intermediates in the early stages of α-synuclein aggregation. Biophys. J. In press; 2012.
[26] Andrekopoulos, C.; Zhang, H.; Joseph, J.; Kalivendi, S.; Kalyanaraman, B. Bicarbonate enhances α-synuclein oligomerization and nitration: intermediacy of carbonate radical anion and nitrogen dioxide radical. *Biochem. J.* **378:**435–447; 2004.
[27] Zhang, H.; Andrekopoulos, C.; Joseph, J.; Crow, J.; Kalyanaraman, B. The carbonate radical anion-induced covalent aggregation of human copper, zinc superoxide dismutase, and α-synuclein: intermediacy of tryptophan- and tyrosine-derived oxidation products. *Free Radic. Biol. Med.* **36:**1355–1365; 2004.
[28] Norris, E. H.; Giasson, B. I.; Ischiropoulos, H.; Lee, V. M. Y. Effects of oxidative and nitrative challenges on α-synuclein fibrillogenesis involve distinct mechanisms of protein modifications. *J. Biol. Chem.* **278:**27230–27240; 2003.
[29] Fancy, D. A.; Kodadek, T. Chemistry for the analysis of protein-protein interactions: Rapid and efficient cross-linking triggered by long wavelength light. *Proc. Natl. Acad. Sci. USA* **96:**6020–6024; 1999.
[30] Fancy, D. A.; Denison, C.; Kim, K.; Xie, Y. Q.; Holdeman, T.; Amini, F.; Kodadek, T. Scope, limitations and mechanistic aspects of the photo-induced cross-linking of proteins by water-soluble metal complexes. *Chem. Biol.* **7:**697–708; 2000.
[31] Nickel, U.; Chen, Y. H.; Schneider, S.; Silva, M. I.; Burrows, H. D.; Formosinho, S. J. Mechanism and kinetics of photocatalyzed oxidation of *p*-phenylenediamines by peroxydisulfate in the presence of tris-2,2'-bipyridilruthenium(II). *J. Phys. Chem.* **98:**2883–2888; 1994.
[32] Herman, L.; Ghosh, S.; Defrancq, E.; Mesmaeker, A. K. D. Ru(II) complexes and light: molecular tools for biomolecules. *J. Phys. Org. Chem* **21:**670–681; 2008.
[33] Gau, B. C.; Chen, H.; Zhang, Y.; Gross, M. L. Sulfate radical anion as a new reagent for fast photochemical oxidation of proteins. *Anal. Chem.* **82:**7821–7827; 2010.
[34] Bosio, G.; Criado, S.; Massad, W.; Nieto, F. J. R.; Gonzalez, M. C.; Garcia, N. A.; Martire, D. O. Kinetics of the interaction of sulfate and hydrogen phosphate radicals with small peptides of glycine, alanine, tyrosine and tryptophan. *Photochem. Photobiol. Sci.* **4:**840–846; 2005.
[35] Pattison, D. I.; Rahmanto, A. S.; Davies, M. J. Photo-oxidation of proteins. *Photochem. Photobiol. Sci.* **11:**38–53; 2012.
[36] Giulivi, C.; Traaseth, N. J.; Davies, K. J. A. Tyrosine oxidation products: analysis and biological relevance. *Amino Acids* **25:**227–232; 2003.
[37] Malencik, D. A.; Sprouse, J. F.; Swanson, C. A.; Anderson, S. R. Dityrosine: preparation, isolation, and analysis. *Anal. Biochem.* **242:**202–213; 1996.
[38] Bitan, G.; Lomakin, A.; Teplow, D. B. Amyloid beta-protein oligomerization—prenucleation interactions revealed by photo-induced cross-linking of unmodified proteins. *J. Biol. Chem.* **276:**35176–35184; 2001.
[39] Bitan, G.; Teplow, D. B. Rapid photochemical cross-linking—a new tool for studies of metastable, amyloidogenic protein assemblies. *Acc. Chem. Res.* **37:**357–364; 2004.
[40] Huang, C. J.; Ren, G. P.; Zhou, H.; Wang, C. C. A new method for purification of recombinant human α-synuclein in *Escherichia coli*. *Protein Expr. Purif.* **42:**173–177; 2005.
[41] Weinreb, P. H.; Zhen, W. G.; Poon, A. W.; Conway, K. A.; Lansbury, P. T. NACP a protein implicated in Alzheimer's disease and learning, is natively unfolded. *Biochemistry* **35:**13709–13715; 1996.
[42] Celej, M. S.; Jares-Erijman, E. A.; Jovin, T. M. Fluorescent *N*-arylaminonaphthalene sulfonate probes for amyloid aggregation of α-synuclein. *Biophys. J.* **94:**4867–4879; 2008.
[43] Tanielian, C.; Wolff, C.; Esch, M. Singlet oxygen production in water: aggregation and charge-transfer effects. *J. Phys. Chem.* **100:**6555–6560; 1996.
[44] Davies, M. J. Singlet oxygen-mediated damage to proteins and its consequences. *Biochem. Biophys. Res. Commun.* **305:**761–770; 2003.
[45] Bayse, G. S.; Morrison, M.; Michaels, A. W. Lactoperoxidase-catalized iodination of tyrosine peptides. *Biochim. Biophys. Acta* **284:**30–33; 1972.
[46] Palecek, E.; Ostatna, V.; Masarik, M.; Bertoncini, C. W.; Jovin, T. M. Changes in interfacial properties of α-synuclein preceding its aggregation. *Analyst* **132:**76–84; 2008.
[47] Doneux, T.; Dorcak, V.; Palecek, E. Influence of the interfacial peptide organization on the catalysis of hydrogen evolution. *Langmuir* **26:** 1347–1353; 2010.
[48] Vetterl, V.; Hason, S. Electrochemical properties of nucleic acid components. In: Palecek, E., Scheller, F., Wang, J., editors. *Electrochemistry of nucleic acids and proteins. Towards electrochemical sensors for genomics and proteomics*. Amsterdam: Elsevier; 2005. p. 18–73.
[49] Palecek, E.; Ostatna, V. Electroactivity of nonconjugated proteins and peptides. Towards electroanalysis of all proteins. *Electroanalysis* **19:**2383–2403; 2007.
[50] Zivanovic, M.; Aleksic, M.; Ostatna, V.; Doneux, T.; Palecek, E. Polylysine-catalyzed hydrogen evolution at mercury electrodes. *Electroanalysis* **22:**2064–2070; 2010.
[51] Wood, S. J.; Wypych, J.; Steavenson, S.; Louis, J. C.; Citron, M.; Biere, A. L. α-Synuclein fibrillogenesis is nucleation-dependent—implications for the pathogenesis of Parkinson's disease. *J. Biol. Chem.* **274:**19509–19512; 1999.
[52] Cookson, M. R. The biochemistry of Parkinson's disease. *Annu. Rev. Biochem.* **74:**29–52; 2005.
[53] Winner, B.; Jappelli, R.; Maji, S. K.; Desplats, P. A.; Boyer, L.; Aigner, S.; Hetzer, C.; Loher, T.; Vilar, M.; Campionic, S.; Tzitzilonis, C.; Soragni, A.; Jessberger, S.; Mira, H.; Consiglio, A.; Pham, E.; Masliah, E.; Gage, F. H.; Riek, R. In vivo demonstration that α-synuclein oligomers are toxic. *Proc. Natl. Acad. Sci. USA* **108:**4194–4199; 2011.
[54] Jang, A.; Lee, H. J.; Suk, J. E.; Jung, J. W.; Kim, K. P.; Lee, S. J. Non-classical exocytosis of α-synuclein is sensitive to folding states and promoted under stress conditions. *J. Neurochem.* **113:**1263–1274; 2010.
[55] Park, J. Y.; Kim, K. S.; Lee, S. B.; Ryu, J. S.; Chung, K. C.; Choo, Y. K.; Jou, I.; Kim, J.; Park, S. M. On the mechanism of internalization of α-synuclein into microglia: roles of ganglioside GM1 and lipid raft. *J. Neurochem.* **110:** 400–411; 2009.
[56] Hansen, C.; Angot, E.; Bergstrom, A. L.; Steiner, J. A.; Pieri, L.; Paul, G.; Outeiro, T. F.; Melki, R.; Kallunki, P.; Fog, K.; Li, J. Y.; Brundin, P. α-Synuclein propagates from mouse brain to grafted dopaminergic neurons and seeds aggregation in cultured human cells. *J. Clin. Invest.* **121:**715–725; 2011.
[57] Cushman, M.; Johnson, B. S.; King, O. D.; Gitler, A. D.; Shorter, J. Prion-like disorders: blurring the divide between transmissibility and infectivity. *J. Cell Sci.* **123:**1191–1201; 2010.
[58] Alvarez-Erviti, L.; Couch, Y.; Richardson, J.; Cooper, J. M.; Wood, M. J. A. Alpha-synuclein release by neurons activates the inflammatory response in a microglial cell line. *Neurosci. Res.* **69:**337–342; 2011.
[59] Danzer, K. M.; Krebs, S. K.; Wolff, M.; Birk, G.; Hengerer, B. Seeding induced by α-synuclein oligomers provides evidence for spreading of α-synuclein pathology. *J. Neurochem.* **111:**192–203; 2009.